Journal of Advanced Research 22 (2020) 7–20

Contents lists available at ScienceDirect

Journal of Advanced Research

journal homepage: www.elsevier.com/locate/jare

Gut butyrate-producing organisms correlate to Placenta Specific 8 protein: Importance to colorectal cancer progression

Chi-Cheng Huang [a,1], Ming-Hung Shen [b,c,d,1], Shao-Kuan Chen [c,e], Shung-Haur Yang [a,f,g], Chih-Yi Liu [h], Jiun-Wen Guo [i,j], Kang-Wei Chang [k,l], Chi-Jung Huang [c,i,j,m,*]

[a] Department of Surgery, Taipei-Veterans General Hospital, Taipei, Taiwan
[b] Department of Surgery, Fu Jen Catholic University Hospital, New Taipei, Taiwan
[c] School of Medicine, College of Medicine, Fu Jen Catholic University, New Taipei, Taiwan
[d] Program in Nutrition and Food Science, Fu Jen Catholic University, New Taipei, Taiwan
[e] Department of Urology, Sijhih Cathay General Hospital, New Taipei, Taiwan
[f] School of Medicine, College of Medicine, National Yang Ming University, Taipei, Taiwan
[g] Department of Surgery, National Yang-Ming University Hospital, Yilan, Taiwan
[h] Department of Pathology, Sijhih Cathay General Hospital, New Taipei, Taiwan
[i] Program in Pharmaceutical Biotechnology, College of Medicine, Fu Jen Catholic University, New Taipei, Taiwan
[j] Department of Medical Research, Cathay General Hospital, Taipei, Taiwan
[k] Isotope Application Division, Institute of Nuclear Energy Research, Taoyuan 32546, Taiwan
[l] Laboratory Animal Center, Taipei Medical University, Taipei 11031, Taiwan
[m] Department of Biochemistry, National Defense Medical Center, Taipei 11490, Taiwan

HIGHLIGHTS

- Genes from stools have molecular significance with CRC tumorgenesis.
- SCFAs, the metabolites of microbiota, can suppress CRC tumorigenesis.
- Relationship between colonic genes, gut microbiota, or their metabolites is significant.
- Changes of PLAC8 and butyrate-producing organisms were found in stools of CRC patients.
- Butyrate can reduce the CRC formation through regulating PLAC8 expression.

GRAPHICAL ABSTRACT

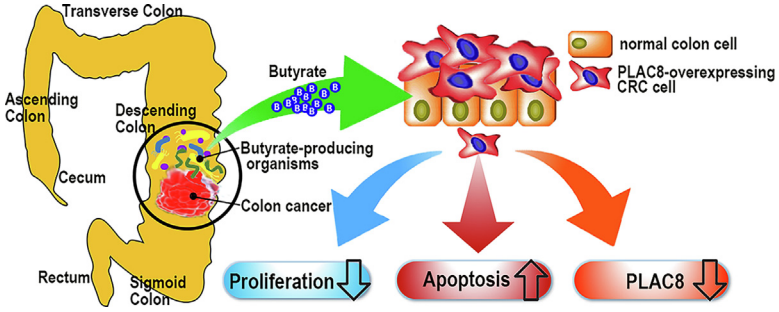

ARTICLE INFO

Article history:
Received 8 September 2019
Revised 29 October 2019
Accepted 12 November 2019
Available online 16 November 2019

Keywords:
Colorectal cancer progression
Gut microbiota
Placenta Specific 8

ABSTRACT

Tumor metastasis or recurrence often occurs in patients with curative resection of colorectal cancer (CRC). Placental-specific 8 (PLAC8), which has increased expression in stool, may be associated with CRC recurrence. Insights into the role of PLAC8 in CRC recurrence and its clinical significance may support to develop strategies for preventing CRC recurrence and deterioration. Clinical tissues, cell and animal models were used to clarify the roles of PLAC8 in CRC tumorigenesis, invasion, and migration. Next-generation sequencing of 16S ribosomal DNA has been used to assess the gut microbiota in stool of CRC patients. We found that PLAC8 was upregulated in tissues from patients with late-stage CRC. In our *in vitro* studies, PLAC8 was dynamically regulated in mitotic cells. Overexpressed PLAC8 was nucleated at the centrosome during mitosis, and therefore, *PLAC8* overexpression might increase cell growth

Peer review under responsibility of Cairo University.
* Corresponding author at: Department of Medical Research, Cathay General Hospital, Taipei, Taiwan.
E-mail address: aaronhuang@cgh.org.tw (C.-J. Huang).
[1] These two authors contributed equally to this manuscript.

https://doi.org/10.1016/j.jare.2019.11.005
2090-1232/

Butyricicoccus
Butyrate

and migration (all $p < 0.05$). The tumorigenic and invasive effects of PLAC8 on CRC cells were also confirmed in a xenograft mouse model. We further identified reduced levels of two butyrate-producing organisms, *Butyricicoccus* and *Prevotella* spp., in stools from CRC patients. We found that butyrate downregulated PLAC8 expression and induced apoptosis in *PLAC8*-overexpressing cells. Our data suggests that PLAC8 gene and protein expression and dysbiosis of gut microflora, especially in butyrate-producing microorganisms, may be indicators of CRC progression.

Introduction

Colorectal cancer (CRC) is a common form of gastrointestinal cancer, and millions of new cases are diagnosed worldwide every year [1,2]. CRC develops slowly through the progressive accumulation of genetic mutations and aberrations in DNA [3]. Despite advances in therapy for CRC patients, 20–45% of those who undergo curative resection subsequently develop tumor relapse or distant metastasis [4,5]. Further, CRC relapse correlates strongly with poor prognosis [4,6,7].

Genes regulating cell growth and differentiation are frequently altered in the process of tumorigenesis in cancerous cells [8]. Patients are increasingly being selected for additional treatment on an individual basis, requiring the identification of indicator molecules whose appearance or activity correlates with CRC relapse or progression [4,9]. Various clinical characteristics and serum markers have recently been identified as risk factors, which can be used to evaluate postoperative relapse and poor prognosis of CRC [10].

Some genes found in human stool samples have been associated with CRC and show molecular significance for cancer biology and molecular medicine [11]. Likewise, molecules involved in tumor progression have been found in the stool of CRC patients [12]. Among those genes, Growth Arrest Specific 2 (*GAS2*, NM_005256) seems to be upregulated in the stool of patients who have relapsed CRC, and its expression has been shown to be affected by targeted chemotherapy [13]. Another gene that might be implicated in tumor progression is Placenta Specific 8 (*PLAC8*, NM_001130715), which has been reported to participate in the epithelial-to-mesenchymal transition (EMT) in CRC [14].

It is thought that some gut microorganisms may affect gene expression in colon cells and possibly the fate of CRC [15,16]. Gut microflora-related mechanisms involved in CRC progression have been identified as new targets for understanding CRC [17,18]. Bacterial dysbiosis in the gastrointestinal tract may induce different molecular mechanisms, which could potentiate development or progression of gastrointestinal tract neoplasms [19]. In addition, metabolites of gut microflora are associated with the inflammatory response. For example, short-chain fatty acids (SCFAs), such as butyrate, can suppress inflammation and tumorigenesis in the gastrointestinal tract [19,20].

Accumulation of aberrant genes may lead to CRC or its progression. Such anomalous genes found in stool, as well as the role of the gut microbiome in CRC development or progression, should be evaluated to determine whether they have clinical relevance [17,19]. We hypothesised that gene expression and gut microflora found in stool may differ between healthy people and patients with CRC, and that this difference may reflect CRC severity. Identifying specific metabolites and/or aberrant human gene expression found in stool may help in devising strategies for the prevention, screening, detection, and treatment of CRC.

In this study, we sought to further understand the role of *PLAC8* in CRC progression and its clinical significance. We used both cell and animal models to clarify the role of *PLAC8* gene and protein expression in CRC invasion, migration, and progression [13]. We immuno-stained tumor sections to evaluate PLAC8 protein expression in tissues from patients with different stages of CRC. Considering the relationship between inflammation and CRC progression, we used next-generation sequencing (NGS) to globally screen for 16S ribosomal DNA (rDNA) in stool samples from patients [16]. To better understand the interactions between gut microflora and colon cells, we examined a metabolite of the gut microflora to determine whether its concentration correlated with the expression of PLAC8 in CRC cells.

Materials and methods

Study participants and animals

Colon tissue sections were obtained from four patients (one non-CRC and three CRC) from Taipei Veterans General Hospital and were used for immunohistochemical (IHC) staining. Twenty-five stool samples were obtained from Cathay General Hospital and were used for NGS of 16S rDNA to study the gut microbiome. The initial tumor stages of these patients were characterized, and three non-CRC controls underwent a colonoscopy examination (Supplementary Table S1). Briefly, the inclusion criteria for enrolled patients were: adult (>20 years old) CRC patients with known AJCC stage, with known clinical characteristics (such as treatment, whether combined with other diseases, smoking or not, and drinking or not), but without diarrhea. The stool samples were presurgically sampled, preserved by snap-freezing, and randomly divided into two groups: a testing group [n = 19: three non-CRC controls, three patients with American Joint Committee on Cancer (AJCC) stage I disease, three with stage II, and ten with stage III/IV (eight were stage III and two were stage IV)]; and a validation group (n = 6: two patients with AJCC stage 0 disease, two with stage II, and two with stage III).

In addition, cDNA arrays of colonic tissues covering four CRC stages (HCRT104; OriGene Technologies) were purchased for quantification of *PLAC8* expression. To examine whether PLAC8 has a tumorigenic effect *in vivo*, a xenograft model was initiated in severe combined immunodeficient (SCID) mice. Ten male SCID mice (CB17/Icr-*Prkdc*^{scid}/IcrIcoCrlBltw) purchased from BioLasco Taiwan Co., Ltd (Taipei, Taiwan) were maintained under specific pathogen-free conditions in an individually ventilated cage rack system (Tecniplast, Varese, Italy) in the Animal Research Center of the Cathay Medical Research Institute, Cathay General Hospital.

16S metagenomics studies using 16S rDNA NGS

Extraction of bacterial DNA from stools was performed according to the protocol in the EasyPrep Stool Genomic DNA kit (Biotools Co., New Taipei, Taiwan). Briefly, an aliquot of stool sample weighing 0.2 g was used. The final extraction resulted in 200 μL of DNA solution, as quantified using a NanoDrop spectrophotometer (Thermo Fisher Scientific, Waltham, MA). We used the Illumina HiSeq sequencing platform (Illumina, San Diego, CA) to analyze 16S rDNA according to the manufacturer's instructions. The sequences of the variable V3 and V4 regions of the 16S rDNA were used for phylogenetic classification, such as genus or species, in

diverse microbial populations [21]. These 250-bp paired-end raw reads derived from the 16S ribosomal amplicon sequencing were assembled using FLASH v.1.2.7 [22]. Bioinformatic analysis was performed for demultiplexing based on barcode identification. As a quality control, reads with a Q score less than the threshold (Q < 20) were discarded in the QIIME 1.7 pipeline [23]. If the quality of three consecutive bases failed to meet the threshold, a truncated read was generated and retained in the data set only if it was ≥75% of the original length [24]. Sequences were chimera-checked using UCHIME to obtain effective tags [25,26] and filtered from the data set before operational taxonomic unit (OTU) clustering at 97% sequence identity using the UPARSE function in the USEARCH v. 7 pipeline [27,28].

For each representative sequence, the RDP classifier (v. 2.2) algorithm was used to annotate the taxonomic classification based on the information retrieved from the Greengenes database (v. 13_8) [29,30]. Sequences with a one-time occurrence (singletons) or that were present in only one sample were filtered out. To analyze the sequence similarities in different OTUs, multiple sequence alignment was conducted using the PyNAST software (v. 1.2) against the core-set dataset in the Greengenes database [31]. In addition, abundance information of OTUs was rarefied to the minimum sequence depth to normalize the variations in sequence depth across samples.

For multivariate statistical analysis, the significance of all species among groups at various taxonomic levels was tested using Metastats software [32]. To identify the community composition in stool, the principal coordinates analysis (PCoA) based on the normalized OTU table was performed to visualize the complex and multidimensional data [33]. A distance matrix using the unweighted UniFrac distances between samples was transformed into a new set of orthogonal axes, in which the most influential variable was represented by the first principal coordinate, and the second most influential one by the second principal coordinate, etc. PCoA analysis was conducted using the WGCNA, stats, and ggplot2 packages in R.

CRC cell lines and gene quantification

Human colon cancer cell lines HCT 116 (ATCC CCL-247; AJCC stage II), LS123 (ATCC CCL-255; AJCC stage II), SW480 (ATCC CRL-1459; AJCC stage II), SW620 (ATCC CRL-1831; AJCC stage III), LoVo (ATCC CCL-229; AJCC stage III), and COLO 205 (ATCC CCL-222; AJCC stage IV) were obtained from the American Type Culture Collection (ATCC; Manassas, VA), and medium suggested for each cell line by the ATCC was used. Primary SW480 cells and lymph node metastatic derivatives (SW620 cells) from the same patient were incubated at 37 °C in 100% air atmosphere (without CO_2) in a humidified incubator.

The total RNA of CRC cells was extracted using RNAzol RT (Molecular Research Center) and converted to cDNA with a High-Capacity cDNA Reverse Transcription Kit in the presence of oligo (dT) primers (Thermo Fisher Scientific) according to the manufacturer's instructions. Gene expression was quantified by qPCR in the presence of specific amplification primers, a TaqMan probe, and TaqMan Master Mix (Roche Diagnostics GmbH, Mannheim, Germany) (Supplementary Table S2) according to the manufacturer's instructions. All mRNA levels were adjusted relative to the level of glyceraldehyde-3-phosphate dehydrogenase to estimate the relative gene expression. LightCycler Software (version 4.05, Roche Diagnostics GmbH) was used to analyze the PCR kinetics.

Evaluation of cell growth and cell migration according to PLAC8 expression

overPLAC8-SW480 cells were used to assess the effect of *PLAC8* on the growth of CRC cells. The relative growth rate was determined by counting cells after different incubation intervals using a Scepter Handheld Automated Cell Counter (Merck KGaA, Darmstadt, Germany). Briefly, cells were counted after different incubation intervals (24, 48, 72 h), and the cell growth rates were expressed relative to the number at the initial seeding. A cell migration experiment with CRC cells that did or did not overexpress *PLAC8* was conducted using a polyethylene terephthalate hanging Transwell insert (diameter, 8 mm) with a pore size of 0.4 μm (PIHT12R48; Merck KGaA) according to our previous publication with minor modifications [13]. Briefly, the times for crystal violet staining were 30 and 60 min for SW480 cells and 20 and 40 min for SW620 cells. The numbers of migrating cells reported here represent the average value ± standard deviation obtained from 2 to 3 independent experiments.

PLAC8 knockdown and overexpression in CRC cells

For *PLAC8* knockdown in SW620 cells, a specific lentivirus-mediated small hairpin (sh) RNA (TRCN0000435105) targeting *PLAC8* (shPLAC8; 5′-GAATGTTGTCCCTGAACTTAG-3′) and a control vector (TRCN0000231719) targeting luciferase (shLUC; 5′-GCGG TTGCCAAGAGGTTCCAT-3′) were acquired from the National RNAi Core Facility of Academia Sinica, Taiwan. Infection of each lentivirus into SW620 cells and selection of stable SW620 cells with shPLAC8 (shPLAC8-SW620) or shLUC (shLUC-SW620) by puromycin and efficacy validation of PLAC8 knockdown were performed. The cDNA fragment encoding PLAC8 was amplified from SW620 cells and cloned into the *Nhe*I and *Pme*I sites of a puromycin-resistant lentiviral vector, pLAS3w.Ppuro (National RNAi Core Facility of Academia Sinica) to induce the overexpression of *PLAC8* in SW480 cells (overPLAC8-SW480). We also amplified GFP from pEGFP-N1 (Takara Bio, Shiga, Japan). Then, GFP/PLAC8 (PLAC8 as a fusion to the C-terminus of GFP) and GFP alone were respectively expressed with pLAS3w.Ppuro in SW620 cells (GFP/PLAC8-SW620 and GFP-SW620). In addition, another lentivector, pLAS3w.RFP-C.Ppuro, which was also purchased from National RNAi Core and that expressed RFP in SW480 cells (RFP-SW480) was used as the expression control. The cloned cDNA fragments in this study were sequenced to confirm their gene identity; Supplementary Table S3 lists the primers used for PCR amplification.

Immunodetection of PLAC8, NF-κB, PARP, and γ-tubulin in cell lines and tissues

To immunodetect target proteins by Western blotting, CRC cell lysates were treated with a protease inhibitor (Hycell, Taipei, Taiwan) and then harvested using the PRO-PREP Protein Extraction Solution (iNtRON Biotechnology, Gyeonggi-do, Korea). Phosphatase Inhibitor Cocktail (Hycell) was added during cell lysate preparation to allow measurement of phosphorylated p65. To localize PLAC8 in the cellular compartment, the cytoplasmic and nuclear protein fractions were extracted and separated using a Nuclear/Cytosol Fractionation Kit (BioVision, Milpitas, CA) according to the manufacturer's instructions. Twenty micrograms of each lysate in 1 × NuPAGE LDS sample buffer (Thermo Fisher Scientific) was denatured (10 min at 95 °C), separated on 12% sodium dodecyl sulfate polyacrylamide gels and transferred to a PolyScreen 2 PVDF Transfer Membrane (0.2 μm; PerkinElmer, Boston, MA). Various target proteins were probed with the following antibodies at the indicated titers: anti-PLAC8 (1:500; ab122652; Abcam, Cambridge, United Kingdom), anti-p65 (1:1000; sc-8008; Santa Cruz Biotechnology, Dallas, TX), anti-phosphorylated p65 (Ser 536) (1:1000; sc-33030; Santa Cruz Biotechnology), anti-PARP (1:1000; #556494; Becton, Dickinson

and Company, Franklin Lakes, NJ), anti-GAPDH (1:5000; AM4300; Thermo Fisher Scientific), anti-α-tubulin (1:1000; sc-5286, Santa Cruz Biotechnology), and anti-lamin A/C (1:500; sc-7292, Santa Cruz Biotechnology) following standard procedures. Different secondary antibodies, either anti-mouse or anti-rabbit, which were conjugated with horseradish peroxidase or alkaline phosphatase, were then used. Blots were finally developed using either Western Lightning Plus-ECL kits for horseradish peroxidase (NEL103E001EA; PerkinElmer) or VECTASTAIN ABC-AmP DuoLuX chemiluminescent/fluorescent substrate kits for alkaline phosphatase (SK-6005; Vector Laboratories, Burlingame, CA) according to the manufacturers' instructions. The images of immunoblots were captured on a FluorChem FC2 system (Cell Biosciences, Santa Clara, CA) and the densitometric ratio of the targeted protein to GAPDH was quantified by FluorChem FC2 as expression level (Version 3.2.2; Cell Biosciences) [34].

To detect PLAC8 in SW480 cells undergoing mitosis, 1×10^5 cells were grown on four-well cell culture slides (SPL Life Sciences, Gyeonggi-do, Korea), rinsed with phosphate-buffered saline (PBS), fixed in 4% paraformaldehyde for 10 min and permeabilized using 0.1% Triton X-100 in PBS for 35 min. Cells were then blocked in a blocking solution (1.5% horse serum in PBS) for 30 min, incubated with anti-PLAC8 (1:50 in blocking solution; 12284-1-AP; Proteintech, Rosemont, IL) at 4 °C overnight, and washed twice with PBS for 5 min. Cells were then probed with a goat anti-rabbit secondary antibody conjugated to Alexa Fluor 488 for 1 h at room temperature in the dark. Next, α-tubulin was fluorescently detected using a protocol similar to that used to detect PLAC8. Briefly, cells on the slides were sequentially hybridized with a primary antibody (1:250 anti-α-tubulin; sc-5286, Santa Cruz Biotechnology) and secondary antibody (1:500 Cy3-conjugated goat anti-mouse; AP124C; Merck KGaA). Both hybridizations were performed at room temperature for 1 h in the dark. Cells were counterstained with 1 μg/ml 4′,6-diamidino-2-phenylindole (DAPI; D9542; Merck KGaA) for 10 min at room temperature to stain the nucleus and finally mounted in a solution of DAPI Fluoromount-G (SouthernBiotech, Birmingham, AL) for imaging with an Eclipse 80i florescence microscope (Nikon Instruments, Melville, NY). Like fluorescently detecting α-tubulin, γ-tubulin was also observed to evaluate centrosome during mitosis. Briefly, the anti- γ Tubulin antibody [TU-30] (1:1000; ab27074, Abcam) and the same Cy3-conjugated secondary antibody were used. In addition, the live-cell images of GFP-SW620 and GFP/PLAC8-SW620 cells were captured by the time-lapse photography of laser scanning confocal microscopy Zeiss LSM 5 PASCAL (Carl Zeiss GmbH, Jena, Germany).

For PLAC8 IHC staining, a VECTASTAIN® Elite ABC kit (Vector Laboratories) was used according to the manufacturer's instructions. Briefly, after deparaffinization, sections were rehydrated sequentially with 100%, 90%, and 70% ethanol. These rehydrated slides were immersed in citrate buffer (10 mM, pH 6.0), boiled (95–99 °C) for 20 min, and cooled to room temperature for 20 min. To inactivate endogenous peroxidases within the tissues, the slides were incubated for 30 min in a 3% H_2O_2 methanolic solution. Tissue sections were then blocked for 30 min with a blocking serum solution (Vector Laboratories) and incubated overnight at 4 °C with an anti-PLAC8 antibody (1:200 in blocking solution; 12284-1-AP; Proteintech). After several washes in Tris-buffered saline, samples were incubated with a biotinylated goat anti-rabbit IgG antibody (1:200 in blocking solution; BA-1000; Vector Laboratories) for 1 h at room temperature. Finally, PLAC8 was visualized with 3,3′-diaminobenzidine (Vector Laboratories) as the substrate. Hematoxylin and eosin (H&E) staining was used to identify non-CRC and CRC areas. PLAC8 and H&E staining were examined and analyzed by pathologists.

Assessment of PLAC8 expression in association with CRC tumorigenesis in vivo

Four-week-old mice were inoculated subcutaneously with 1×10^6 SW620 cells/0.2 ml PBS without or with *PLAC8* knockdown on the right side of the back. These different SW620 cells also coexpressed the luciferase gene, which was cloned from the pGL3-Basic vector (Promega, Madison, WI) and subcloned into pLAS3w.Pbsd, a lentiviral vector with blasticidin resistance (National RNAi Core Facility of Academia Sinica). Sequences of primers were shown in Supplemental Table S3.

To track the growth of xenografts in mice using luciferase imaging, D-luciferin (Biosynth, Staad, Switzerland) at a concentration of 1.5 mg/10 g body weight was injected intraperitoneally into mice, and luciferase imaging (Xenogen IVIS-200, PerkinElmer) was used 10 min later to image the whole mouse. These images were analyzed further and quantified using Living Image 3.0 software (PerkinElmer). The size of xenografts was assessed by calculating the tumor volume (cm^3) using the following formula: volume = (width^2-$\times$ length)/2 [35]. In addition, positron emission tomography (PET) and computed tomography (CT) were used to detect distant metastases of xenografts in SCID mice, as described by Jensen et al. with minor modifications [21], and as described below.

PET and CT

Mice were injected with 0.5 mCi (18.5 MBq) 18F-fluorodeoxyglucose following 12-hour starvation. One hour after tracer injection, mice were anesthetized with 2% isoflurane (Piramal Critical Care, Bethlehem, PA) mixed with 35% O_2 in N_2 and fixed on a bed in the presence of three fiducial markers to allow combined PET and CT images. A 10-minute PET scan was acquired using a nanoScan PET/CT (Mediso, Budapest, Hungary). After data acquisition, PET data were arranged into sinograms and subsequently reconstructed with the maximum a posteriori reconstruction algorithm. The pixel size was $0.8666 \times 0.8666 \times 0.7960$ mm^3, and the resolution was 1.4 mm full-width-at-half-maximum in the center field of view. Following the nanoPET scan, a 10-minute nanoCT scan was performed with the following parameter settings: 360 rotation steps, tube voltage 60 kV, tube current 500 mA, binning 4, and exposure time 310 ms. The pixel size was $0.0916 \times 0.0916 \times 0.0910$ mm^3. The nanoPET and nanoCT images were fused using InVivoScope software (BioScan, Oxnard, CA). Finally, the mice were euthanized and xenografts that grew subcutaneously on the back and metastatic tissues were removed and snap frozen for DNA genotyping using a GlobalFiler Express PCR Amplification Kit according to the manufacturer's instructions (Thermo Fisher Scientific).

Statistical analysis

Differences in the growth rates and migration potential according to *PLAC8* expression and the relative levels of *PLAC8* expression were compared between samples using Student's *t* test or the Mann–Whitney *U* test. All statistical analyses were performed using SPSS software (13.0; SPSS Inc., Chicago, IL). $p < 0.05$ was considered to be significant.

Results

Taxonomy-based comparisons of intestinal microflora among non-CRC controls and CRC patients

The NGS datasets of 16S rDNA were deposited in the Sequence Read Archive (accession code: PRJNA545850) of National Center for

Biotechnology Information, U.S. National Library of Medicine. In the analysis of the microbial community composition of the stools and PCoA based on unweighted UniFrac distances of the 16S rDNA revealed that samples from patients with late-stage CRC (AJCC stages III and IV) differed from the three other groups (non-CRC controls, patients with AJCC stage I or II disease) (Fig. 1A). In the PCoA plot, microbial communities were separated according to AJCC staging. Annotation at the phylum and family levels revealed variability in the relative abundance of the top 10 species. Notably, the percentages of Bacteroidetes, Firmicutes, Proteobacteria, and Fusobacterium spp. of the total phyla were up to 99.0% in each patient group, as indicated in Fig. 1B. By contrast, the family

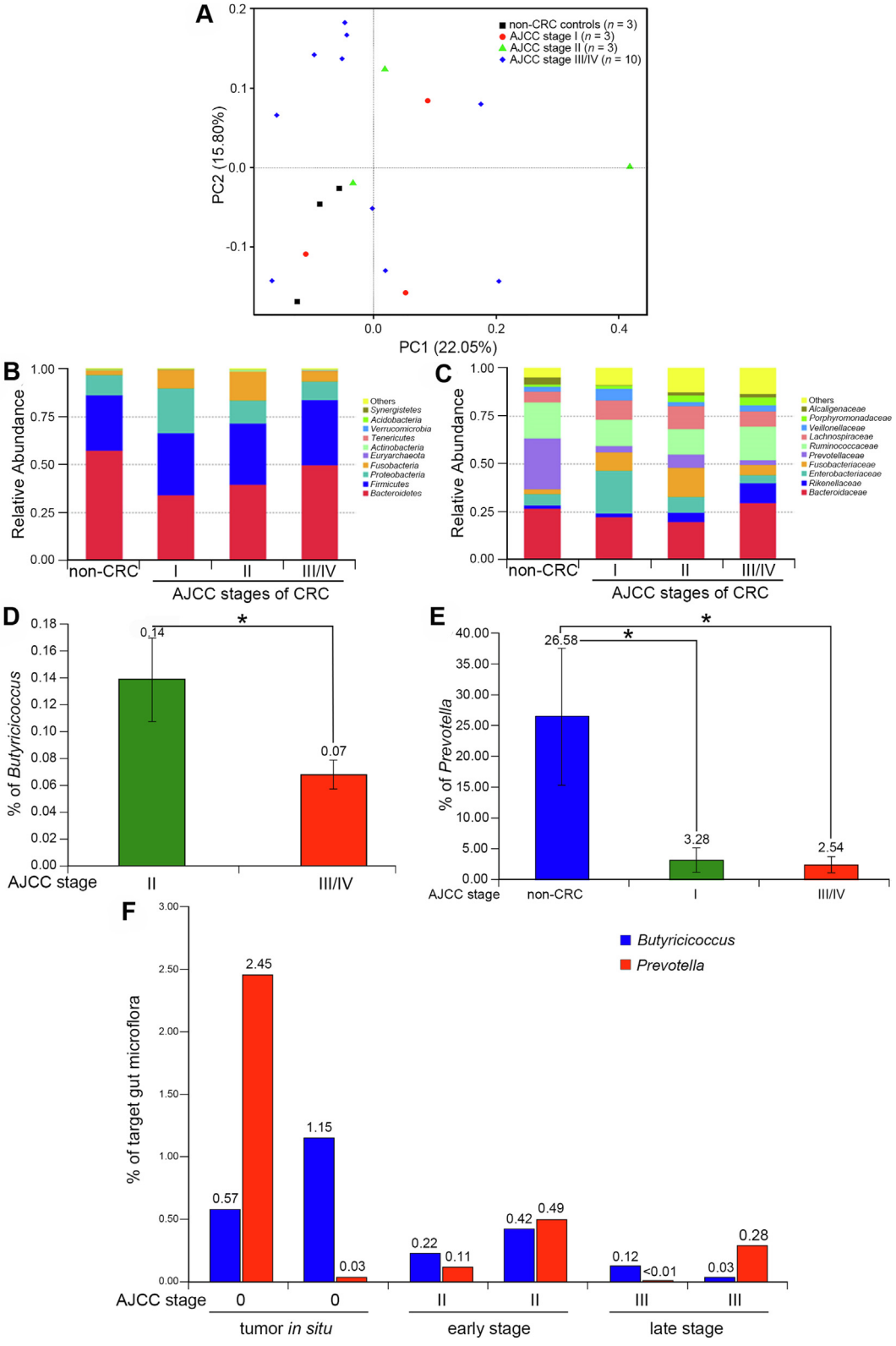

Prevotellaceae (control: 26.6%; AJCC stage I: 3.3%; stage II: 6.9%; stages III and IV: 2.5%), which is the butyrate-producing organism, decreased with progressive CRC stages (Fig. 1C).

We next focused on the butyrate-producing microflora with lower percentages in the stool of patients with late-stage CRC. We were interested in whether the lower percentages correlated with colon tumor growth. For all genera of gut microflora sequenced, *Butyricicoccus* and *Prevotella* had lower percentages in stool from CRC patients compared with the other groups. As shown in Fig. 1D, the percentage of *Butyricicoccus* was significantly lower in the stools of patients with stage III/IV disease (0.068% ± 0.011%; $p = 0.032$) compared with patients with stage II disease (0.140% ± 0.031%). In addition, *Prevotella* of the non-CRC controls represented about 26.583% ± 11.113% of the total genera; but this percentage was markedly lower in the stools of patients with stage I disease (3.277% ± 1.963%; $p = 0.048$) or stage III/IV disease (2.539% ± 1.308%; $P = 0.044$) (Fig. 1E).

We examined further the significance of *Butyricicoccus* and *Prevotella* spp. in the validation group, which included six CRC patients. As shown in Fig. 1F, the percentage of *Butyricicoccus* was markedly higher in patients with stage 0 disease than in those with other disease stages. In particular, two patients with late-stage disease (AJCC stage III/IV) had minimal *Butyricicoccus* in their stools. Similarly, the percentages of *Prevotella* showed a decreasing trend with increasing disease stage. The lowest amount of *Prevotella* was detected in the stool of one patient with late-stage disease. We used the OTU to compare gut microbial percentages in stools from CRC patients and healthy controls. Among all of the bacterial groups studied at the species level, compared with healthy controls, the percentage for a major lactate-producing member of the gut microbiome, *Bifidobacterium longum* (*B. longum*), was significantly lower in patients with different stages of CRC: 16.5% for AJCC stage I ($p = 0.019$); 20.0% for stage II ($p = 0.014$); and 20.6% for stage III ($p = 0.010$) (Table 1).

Table 1
Comparison of *Bifidobacterium longum* in stool samples of non-CRC controls and CRC patients.

	Relative % of *Bifidobacterium longum* (CRC *vs.* non-CRC controls)	*p*
Patients with AJCC stage I	16.5%	0.019
Patients with AJCC stage II	20.0%	0.014
Patients with AJCC stage III/IV	20.6%	0.010

Non-CRC controls, $n = 3$; patients with AJCC stage I, $n = 3$; patients with AJCC stage II, $n = 3$; patients with AJCC stage III/IV, $n = 10$ (eight were stage III and two were stage IV).

Variations of colon cells caused by butyrate and PLAC8

As detailed above, we found that the abundance of some butyrate-producing organisms was reduced in the stool of CRC patients with late-stage disease. We treated CRC cell lines with 5 mM sodium butyrate (NaB) for 24 h. PLAC8, which is highly expressed in many late-stage CRC cell lines (SW620 cells, LoVo cells and COLO 205 cells) (Fig. 2A), was significantly downregulated at the messenger RNA (mRNA) levels (Fig. 2B for SW620 cells, Fig. 2C for LoVo cells, and Fig. 2D for COLO 205 cells). The differential expression of endogenous PLAC8 in SW480 cells, SW620 cells or from treating cells with NaB (Fig. 2E) was confirmed by the immunodetection of an anti-PLAC8 antibody. Briefly, NaB-treated SW620 cells expressed lower levels of PLAC8 (0.8 folds), relative to cells without NaB treatment (1.0-fold, right panel of Fig. 2I). Malignant SW620 cells were next used to study the tumorigenic potential of *PLAC8* and anti-tumorigenic behavior of NaB in CRC.

These findings suggest that decreases in PLAC8 expression in CRC cells after exposure to NaB may alter the fate of those cells. First, we found the growth rate of SW620 cells was attenuated after NaB treatment. Second, compared with cell growth without NaB, SW480 and SW620 cell numbers decreased after NaB treatment (Fig. 2F). NaB (5 mM) had a significant effect on the growth of SW620 cells (18.5% for 48 h and 2.8% for 72 h), but a smaller effect on the growth of SW480 cells (34.7% for 48 h and 6.0% for 72 h).

Next, we found that the migration rate of SW620 cells was impaired by NaB. Specifically, the number of cells that migrated through the membrane of the Transwell inserts was markedly reduced in the presence of 5 mM NaB (Fig. 2G). There was a significant difference in the migration of SW620 cells after treating cells with 5 mM NaB for 60 min (Fig. 2H).

We also examined PLAC8-specific reduction caused by NaB treatment in changing apoptotic and cell proliferation markers. Knockdown of *PLAC8* decreased the protein level to less than 0.1-fold in SW620 cells (shPLAC8-SW620), compared to control cells (shLUC-SW620) (Fig. 2I). Similar to Fig. 2E, NaB treatment resulted in a reduction of PLAC8 in shLUC-SW620 cells by 0.7-fold (Fig. 2I). A cleaved poly (ADP-ribose) polymerase (PARP) fragment (indicated by red arrowhead in Fig. 2I) was detected in NaB (5 mM)-treated shLUC-SW620 cells (12.3 folds), but no cleaved band was observed in shPLAC8-SW620 cells (1.0 fold). We also measured the mRNA levels of the genes for proliferating cell nuclear antigen (*PCNA*) and Ki-67 (*MKI67*) in SW620 cells (Fig. 2J). Both were downregulated in cells treated with 5 mM NaB. However, we found NaB had no effect on the expression of these genes in NaB-treated shPLAC8-SW620 cells (Fig. 2K).

Elevated expression of PLAC8 in CRC tissues and CRC cells

Differential expression of *PLAC8* in stool samples was also detected in CRC tissues.[12,36] We first confirmed the effect of differential expression on mRNA levels in complementary DNA (cDNA) samples from CRC patients with four AJCC stages. *PLAC8* was expressed at a significantly higher level in cDNA samples from metastatic patients (AJCC stage III/IV, $n = 25$) than in patients with

Fig. 1. Taxonomy-based comparisons of intestinal microflora among non-CRC controls and CRC patients. (**A**) PCoA scores plot based on the relative abundance of OTUs (97% similarity level). Unweighted UniFrac distance matrices were generated to analyze the differences in the overall bacterial diversity across the samples. Each symbol represents a sample. Black square, non-CRC controls; Red circle, CRC patients with AJCC stage I; Green triangle, CRC patients with stage II; Blue diamond, CRC patients with stage III or IV. PCoA, principal coordinate analysis; OTU, operational taxonomic unit. (**B**) Relative abundance of dominant bacterial phyla in stools. (**C**) Relative abundance of dominant bacterial families in stools. Histogram represents the relative abundance of different bacteria from non-CRC controls ($n = 3$) and CRC patients [$n = 16$: three with AJCC stage I; three with stage II; ten with stage III/IV (eight were stage III and two were stage IV)]. "Others" represents the unclassified bacteria. (**D**) Percentage of *Butyricicoccus* genus in stools of CRC patients with AJCC stages II, III, and IV. (**E**) Percentage of *Prevotella* genus in stools of non-CRC controls and CRC patients with AJCC stages I, III, and IV. These percentages were determined by relative to the total detected OTUs in each stool sample. Error bars showed standard deviation. The statistical significance was calculated with Student's *t* test (*$p < 0.05$). (**F**) Percentages of *Butyricicoccus* and *Prevotella* spp. in stools of the validation group. The individual percentage was indicated at the top of each sample [two with stage 0 (tumor in situ), two with early stage (AJCC stage II), and two with late stage (AJCC stage III)]. Relative abundance, the relative amount of each phylum or family to the total number of gut microbes in the level of classification. (For interpretation of the references to colour in this figure legend, the reader is referred to the web version of this article.)

non-metastatic disease (AJCC stage I/II: $n = 13$, $p < 0.05$) (Fig. 3A). These differences in mRNA levels were also reflected in the respective protein expression levels. PLAC8 protein stained intensely in CRC tissues of patients with AJCC stage III disease, and weakly in the non-CRC sample and in those from patients with non-metastatic CRC (AJCC stage II in Fig. 3B). Detailed views of the PLAC8 protein localisation in the cytoplasmic compartment are shown in Fig. 3B insets. Shown with the online tools of

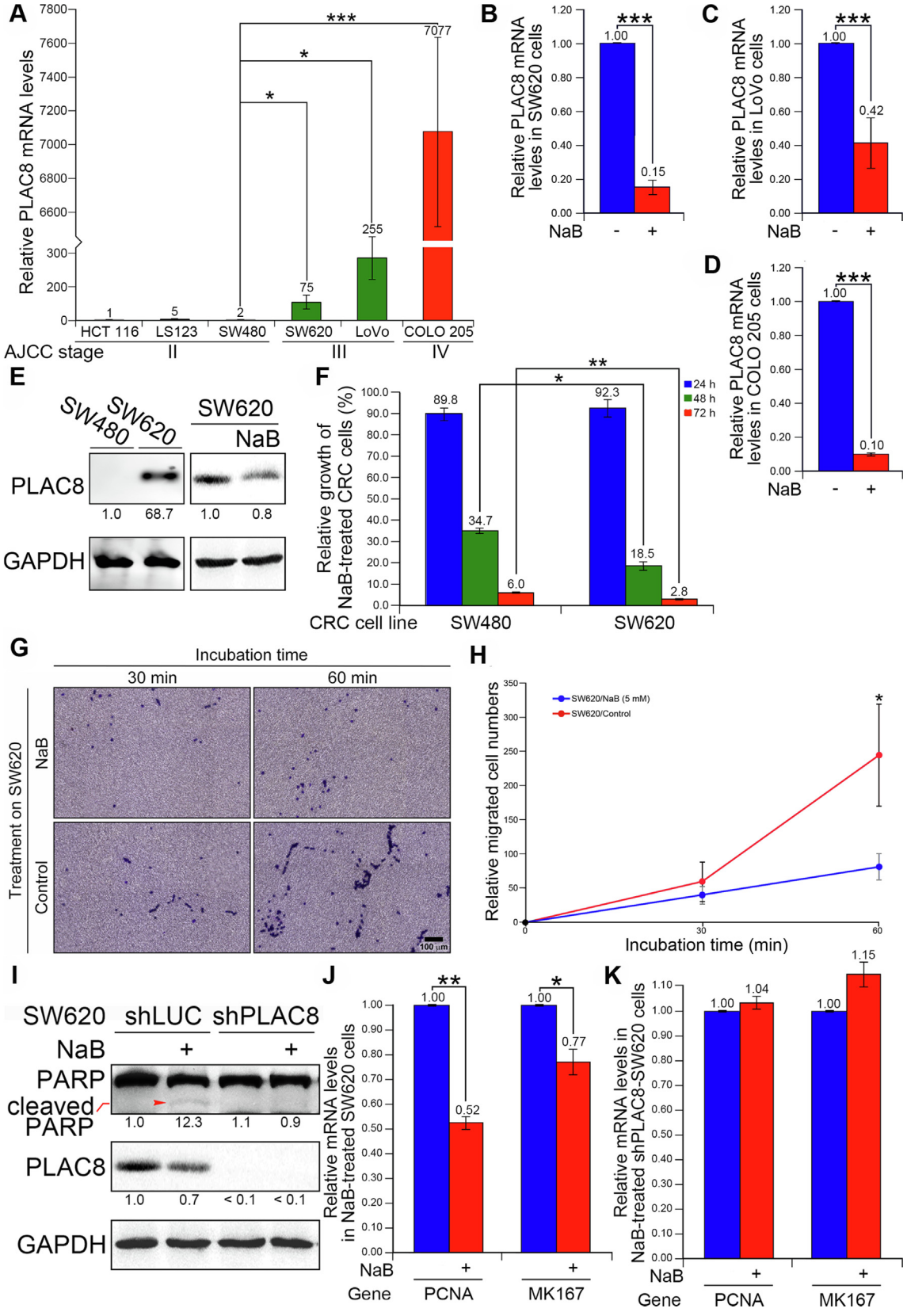

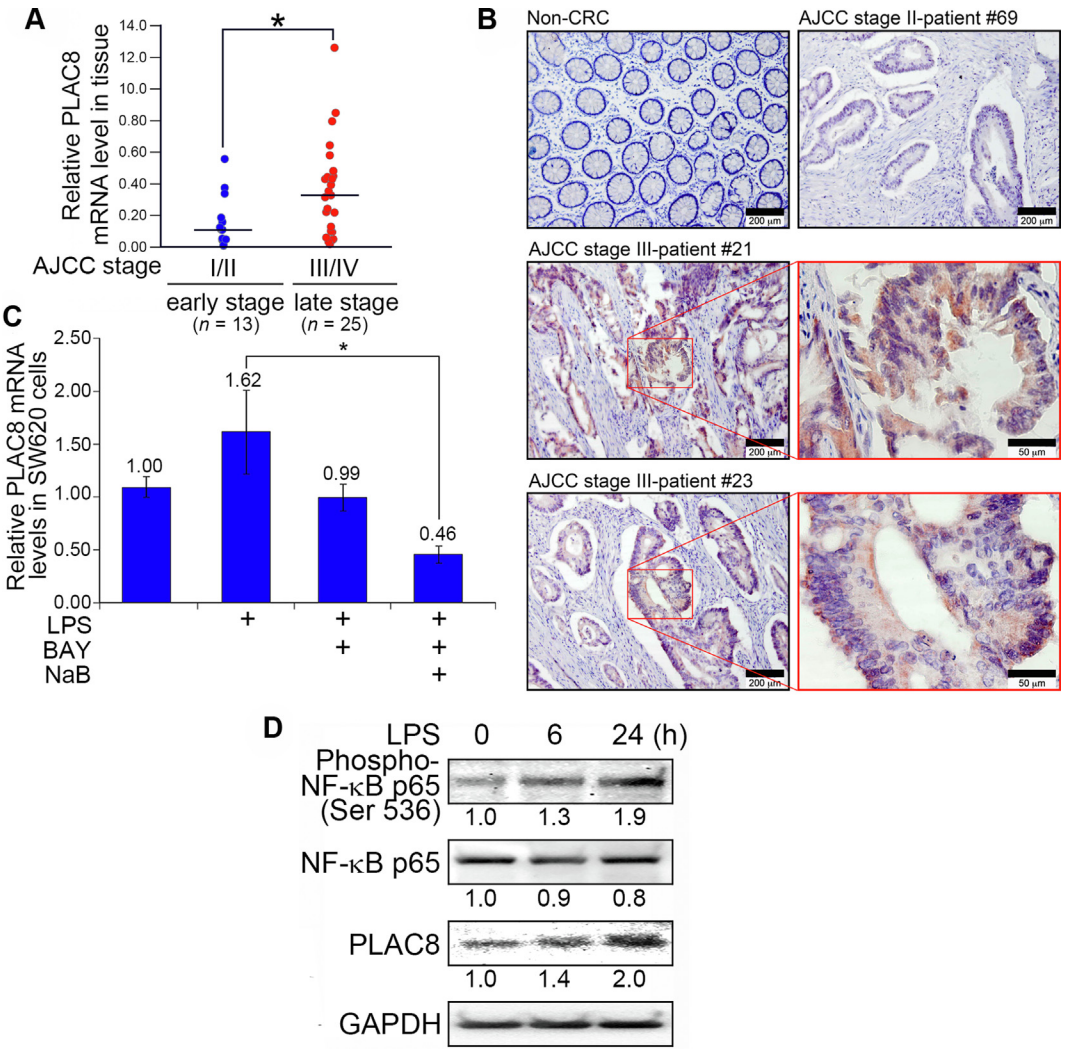

Fig. 3. Elevated expression of PLAC8 in CRC tissues and CRC cells. (A) Relative mRNA level of *PLAC8* in CRC tissues. cDNA samples were acquired from colonic tissues covering four CRC stages (HCRT104; OriGene Technologies). The case numbers and clinical stages were indicated. *PLAC8* expression was quantified by quantitative real-time reverse transcription polymerase chain reaction and relative to the expression of glyceraldehyde-3-phosphate dehydrogenase (*GAPDH*). The line within each group indicated the median level. The statistical significance was calculated with Mann-Whitney *U* test (*$p < 0.05$). (**B**) Immunohistochemistry of PLAC8 in colonic tissue sections. Representative images were from one non-CRC control and three CRC (one with AJCC stage II and two with AJCC stage III) tissue sections. Relative insets from two patients with AJCC stage III were illustrated with red box. Scale bars, 200 μm for representative images and 50 μm for insets. (**C**) Reduction of *PLAC8* expression by NF-κB inhibitor in SW620 cells. cDNA samples were acquired from SW620 cells with different treatments for 24 h. *PLAC8* expression of each condition was relative to the level of PLAC8 of Human Reference cDNA (qPCR Human Reference cDNA, oligo(dT)-primed; Takara Bio USA). LPS, lipopolysaccharide; BAY, NF-κB inhibitor BAY 11-7082; NaB, sodium butyrate. Error bars showed standard deviation obtained from 2 to 3 independent experiments. The statistical significance was calculated with Student's *t* test (*$p < 0.05$). (**D**) Immunodetection of proteins from LPS-treated SW620 cells. Cell lysates were prepared from SW620 cells with different LPS-treated time as indicated. Protein levels of PLAC8, NF-κB p65, and phosphorylated NF-κB p65 (Ser 536) were determined by western blotting. (For interpretation of the references to colour in this figure legend, the reader is referred to the web version of this article.)

Fig. 2. Variations of colon cells caused by butyrate and PLAC8. (A) Relative *PLAC8* expressions in different CRC cell lines. *PLAC8* expression was quantified by quantitative real-time reverse transcription polymerase chain reaction (qPCR) and relative to the expression of glyceraldehyde-3-phosphate dehydrogenase (*GAPDH*). cDNA samples were acquired from CRC cell lines with AJCC stage II (HCT 116, LS123, and SW480), stage III (SW620 and LoVo), and stage III (COLO 205). (**B**) mRNA level of PLAC8 was reduced in NaB-treated SW620 cells. (**C**) mRNA level of PLAC8 was reduced in NaB-treated LoVo cells. (**D**) mRNA level of PLAC8 was reduced in NaB-treated COLO 205 cells. cDNA samples were acquired from CRC cells without or with 5 mM NaB treatment. (**E**) Immunodetection of PLAC8 in SW480 and SW620 cells. SW620 cells were further treated with 5 mM NaB. The protein level of GAPDH was used as a loading control. (**F**) Different growth of SW480 and SW620 cells under NaB treatment. Cells were treated with 5 mM NaB for different time (blue bar, 24 h; green bar, 48 h; red bar, 72 h). All growth rates were relative the cell numbers at initial culture (0 h). (**G**) Representative images of migrated SW620 cells under NaB treatment. All migrated cells were evaluated using a polyethylene terephthalate hanging cell culture insert with 0.4 μm pores. The filter membrane was removed, fixed with methanol, and stained with crystal violet. Migrated cells were detected at 30 and 60 min after adding 5 mM NaB. Control, cells without 5 mM NaB treatment; NaB, cells with 5 mM NaB treatment; NaB, sodium butyrate. Scale bar, 100 μm. (**H**) Relative migrated cell numbers of SW620 cells under NaB treatment. Cells were treated without (Control, red line) or with (5 mM NaB, blue line) for different time. The numbers of migrated SW620 cells were counted in three-to-four random fields under a light scope. (**I**) Changes of protein levels in accordance with NaB treatment. Cell lysates were prepared from shLUC-SW620 cells and shPLAC8-SW620 cells. Red arrowhead indicated the cleaved PARP band. PARP, poly(ADP-ribose) polymerase; shLUC, targeting luciferase and normally express *PLAC8*; shPLAC8, PLAC8 knockdown. (**J**) Relative mRNA levels of cell proliferation markers from SW620 cells. (**K**) Relative mRNA levels of cell proliferation markers from shPLAC8-SW620 cells. Blue bar, cells without NaB treatment; red bar, cells with (+) 5 mM NaB treatment. All mRNA levels were relative to the level of *GAPDH* and were compared to the relative level of cells without NaB treatment. Blue bar, cells without NaB treatment; red bar, cells with (+) 5 mM NaB treatment. *PLAC8*, Placenta Specific 8; *PCNA*, Proliferating Cell Nuclear Antigen; MK167, Marker of Proliferation Ki-67. Error bars showed standard deviation obtained from 2 to 3 independent experiments. The statistical significance was calculated with Student's *t* test (*$p < 0.05$; **$p < 0.01$; ***$p < 0.001$). (For interpretation of the references to colour in this figure legend, the reader is referred to the web version of this article.)

transcription factor binding sites (http://www.sabiosciences.com/chipqpcrsearch.php?app = TFBS), nuclear factor-κB (NF-κB), which is involved in the proinflammatory response, is thought to transactivate the expression of *PLAC8* via a site-specific mechanism [37]. We found that the transactivation of *PLAC8* occurred in SW620 cells after treatment with the inflammatory mediator lipopolysaccharide (LPS). As shown in Fig. 3C, compared with untreated cells, the relative mRNA level of *PLAC8* was increased by 1.62-fold after treatment with LPS for 24 h. Like the results from the quantitative real-time reverse transcription polymerase chain reaction (qPCR), the immunoblots showed that LPS induced phosphorylation of p65 (a subunit of the NF-κB transcription complex) and increased PLAC8 protein content. The average density value for PLAC8 (1.4 for 6 h and 2.0 for 24 h) in LPS treated SW620 cells increased with NF-κB phosphorylation (1.3 for 6 h and 1.9 for 24 h) (Fig. 3D). However, the increase in *PLAC8* mRNA levels caused by LPS was attenuated in the presence of the NF-κB inhibitor BAY 11-7082, or significantly decreased if cells were co-treated with BAY 11-7082 and NaB (Fig. 3C).

Cell growth changes in the presence of upregulated PLAC8 were observed in vitro and in vivo

As depicted in Fig. 4A, growth of *PLAC8*-overexpressing SW480 (overPLAC8-SW480) cells increased steadily compared to SW480 cells expressing red fluorescent protein (RFP; RFP-SW480 cells). Moreover, overPLAC8-SW480 cells grew faster than the control SW480 cells and the RFP-SW480 cells, and the difference in growth was significant for cells incubated for 48 h or 72 h (all $p < 0.05$).

OverPLAC8-SW480 cells also exhibited an increased migration rate relative to cells without overexpressed *PLAC8* (RFP-SW480 cells), as indicated by positive crystal violet staining of the cells migrating through pores to the underside of the membrane (Fig. 4B). The number of migrated cells approached a significantly higher amount for overPLAC8-SW480 cells compared to RFP-SW480 cells ($P = 0.087$) (Fig. 4C). Moreover, the migration ability of SW620 cells was decreased by knockdown of *PLAC8* expression (Fig. 4D and 4E; $p < 0.05$). In addition, the expressions of genes *PCNA* and *MKI67* (which promote tumor growth), the marker of intestinal stem cells (*LGR5*), and an EMT marker (*EPHB2*) were all downregulated in shPLAC8-SW620 cells relative to those in control cells (shLUC-SW620) (Fig. 4F).

The changes in CRC cell growth and migration in response to *PLAC8* expression *in vitro* were also detected *in vivo*. In the animal study, the xenograft tumor size induced by grafting of shLUC-SW620 cells, which normally express *PLAC8*, was markedly larger than that in tumors derived from shPLAC8-SW620 cells. As Fig. 4G illustrates, shLUC-SW620 cells grew significantly faster on the back of SCID mice, based on luciferase imaging. The highest signal was found in SCID mice inoculated with shLUC-SW620 cells and cultured for 34 days, while mice inoculated with shPLAC8-SW620 cells had lower signals. Tumor size differed significantly between tumors induced with and without *PLAC8* knockdown. Fig. 4H shows that xenograft tumors were significantly larger when derived from shLUC-SW620 cells than from shPLAC8-SW620 cells ($p < 0.05$). Moreover, shLUC-SW620 cells migrated from the primary site, where cancer cells had been injected subcutaneously and metastasised distantly to the lungs (Fig. 4I). The tumor lesions in the lung (indicated by a red arrowhead in Fig. 4J) were harvested from a SCID mouse that had received subcutaneous inoculation of shLUC-SW620 cells. The genotype of SW620 cells was determined in the tumors at sites of local subcutaneous inoculation and distant metastasis (Supplementary Fig. S1).

Expression and translocation of PLAC8 in CRC cells undergoing cell division

Immunoblotting (Fig. 5A) and immunofluorescence detection (Fig. 5B) showed that PLAC8 localized to the cytoplasm in SW620 cells. SW480 cells expressed less PLAC8 if they did not undergo cell division. The expression of PLAC8 in parental SW480 cells was induced dynamically in cells undergoing mitosis, but the cells were negative for PLAC8 at interphase. As shown in Fig. 5C, PLAC8 staining began to increase at prophase, reached a peak at metaphase, and then decreased gradually until the cells were in cytokinesis during the mitotic cycle. We next overexpressed PLAC8 as part of the fusion protein, green fluorescent protein (GFP)/PLAC8, in SW620 cells, which appeared to disengage followed by its nucleation and reduplication and then gradual migration to opposite poles of the mitotic cell (Fig. 5D, the

Fig. 4. Cell growth changes in the presence of upregulated PLAC8 *in vitro* and *in vivo*. (**A**) Growth of SW480 cells in accordance with PLAC8 expression. All growth curves were relative the cell numbers at initial culture (0 h). SW480 (green line), parental SW480 cells; RFP-SW480 (blue line), SW480 cells infected with pLAS3w.RFP-C.Ppuro which expressed RFP as control infection; overPLAC8-SW480 (red line), SW480 cells infected with PLAC8-containing pLAS3w.Ppuro which overexpressed PLAC8. The statistical significance was calculated with Student's *t* test (*$p < 0.05$). (**B**) Representative images of migrated SW480 cells in accordance with PLAC8 expression. All migrated cells were evaluated using a polyethylene terephthalate hanging cell culture insert with 0.4 μm pores. The filter membrane was removed, fixed with methanol, and stained with crystal violet. Migrated cells were detected after culturing cells for 30 and 60 min. Scale bar, 100 μm. (**C**) Relative migrated cell numbers of SW480 cells in accordance with PLAC8 expression. RFP, cells without overexpressed PLAC8 (blue line) or overexpressed PLAC8 (overPLAC8, red line). Migrated cells were counted after culturing cells for 30 and 60 min in three-to-four random fields under a light scope. The statistical significance was calculated with Student's *t* test (#$p < 0.1$). (**D**) Representative images of migrated SW620 cells in accordance with PLAC8 expression. shLUC, targeting luciferase and normally express *PLAC8*; shPLAC8, PLAC8 knockdown. All migrated cells were evaluated and stained as SW480 cells with the exception of the detecting time (20 and 40 min). Scale bar, 100 μm. (**E**) Relative migrated cell numbers of SW620 cells in accordance with PLAC8 expression. shPLAC8, blue line; shLUC, red line. Migrated cells were counted after culturing cells for 20 and 40 min in three-to-four random fields under a light scope. The statistical significance was calculated with Student's *t* test (*$p < 0.05$). (**F**) Relative mRNA levels of genes in shPLAC8-SW620 cells. All mRNA levels were relative to the level of glyceraldehyde-3-phosphate dehydrogenase and were compared to the relative level of shLUC-SW620 cells. Blue bar, shLUC620 cells; red bar, shPLAC8 cells. *PLAC8*, Placenta Specific 8; *PCNA*, Proliferating Cell Nuclear Antigen; *MK167*, Marker of Proliferation Ki-67. *EPHB2*, EPH Receptor B2; *LGR5*, Leucine Rich Repeat Containing G Protein-Coupled Receptor 5. The statistical significance was calculated with Student's *t* test (*$p < 0.05$; **$p < 0.01$). Data are mean ± s.d. (**G**) Growth of xenograft tumor in accordance with PLAC8 expression. Four-week-old SCID mice were inoculated subcutaneously with 1×10^6 shLUC-SW620 cells or shPLAC8-SW620 cells on the right side of the back. Representative IVIS images demonstrated the tumor growth at the day post injection as indicated. IVIS, Non Invasion In Vivo Imaging System. (**H**) Size of xenograft tumor in accordance with PLAC8 expression. The dimensions of injection sites were measured roughly at the indicated time points while study. Tumor volumes (mm^3) were calculated as described in Methods. shLUC-SW620 cells, red line; shPLAC8-SW620 cells, blue line. (**I**) Representative nanoPET/CT images in accordance with PLAC8 expression. A 10-minute PET scan was acquired after injection and one-hour distribution of F-18-FDG using a nanoScan PET/CT. The nanoPET and nanoCT images were fused. The left panel shows higher tracer uptake in the lung, heart, and bladder, but the right panel shows higher tracer uptake only in the heart and bladder. PET, positron emission tomography; CT, computed tomography. L, left side view; R, right side view. (**J**) Lung tissues of SCID mice in accordance with PLAC8 expression. Mice with xenograft tumors were euthanized and the lung organs were removed. The black arrowheads indicated the sites of metastatic tumors. Error bars showed standard deviation obtained from 2 to 3 independent experiments or from 3 to 5 mice for size of xenograft tumor. The statistical significance was calculated with Student's *t* test (*$p < 0.05$). (For interpretation of the references to colour in this figure legend, the reader is referred to the web version of this article.)

lower panel). In contrast, GFP alone in SW620 cells did not show the same migration (Fig. 5D, the upper panel). We also found that the GFP/PLAC8 fusion protein was accompanied by γ-tubulin at the centrosome of mitotic cells during interphase and metaphase (Fig. 5E).

Discussion

CRC is a heterogeneous disease, which develops from proximal and distal colon cells with a distinct genetic signature [38]. Identifying and detecting the molecules involved in or associated with

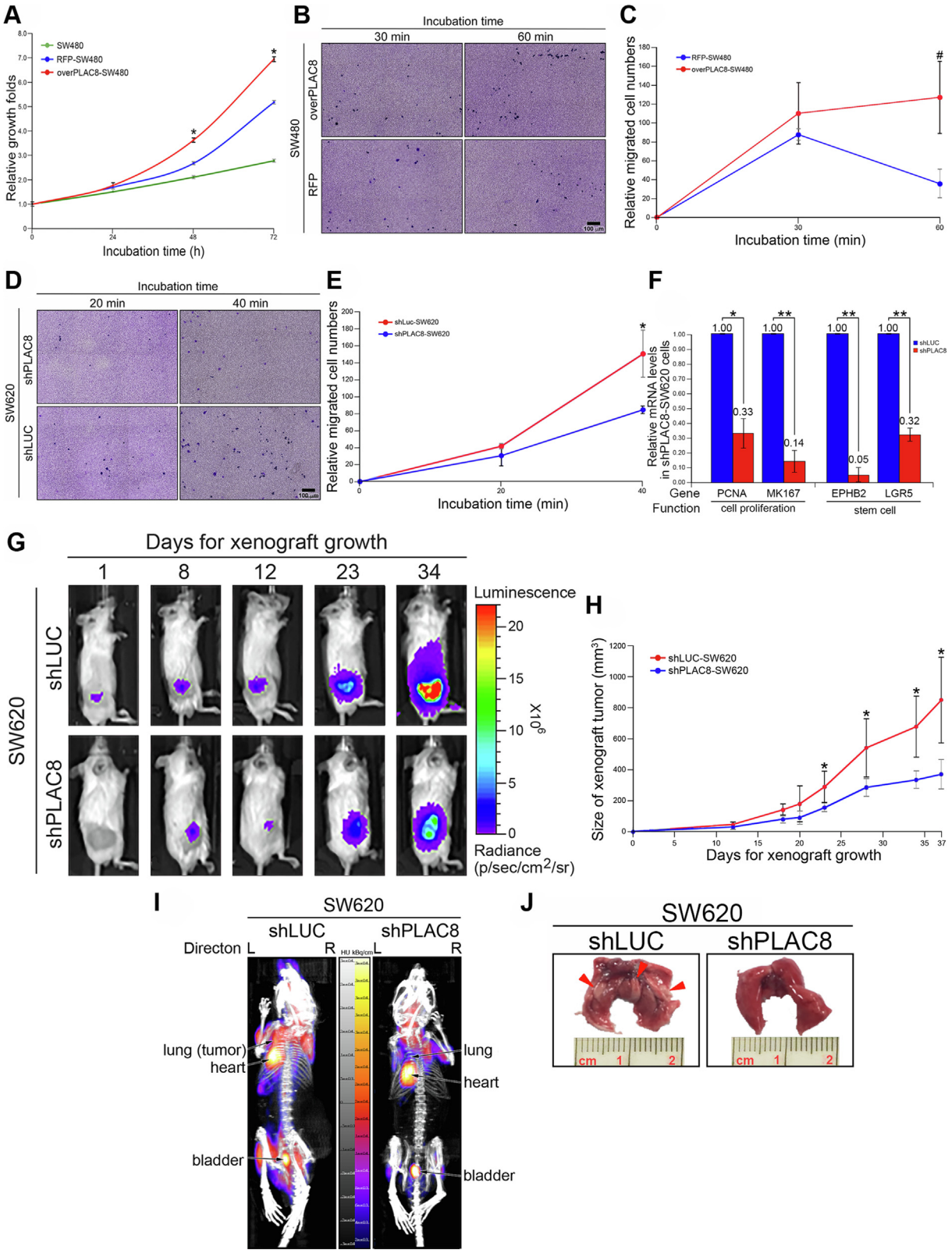

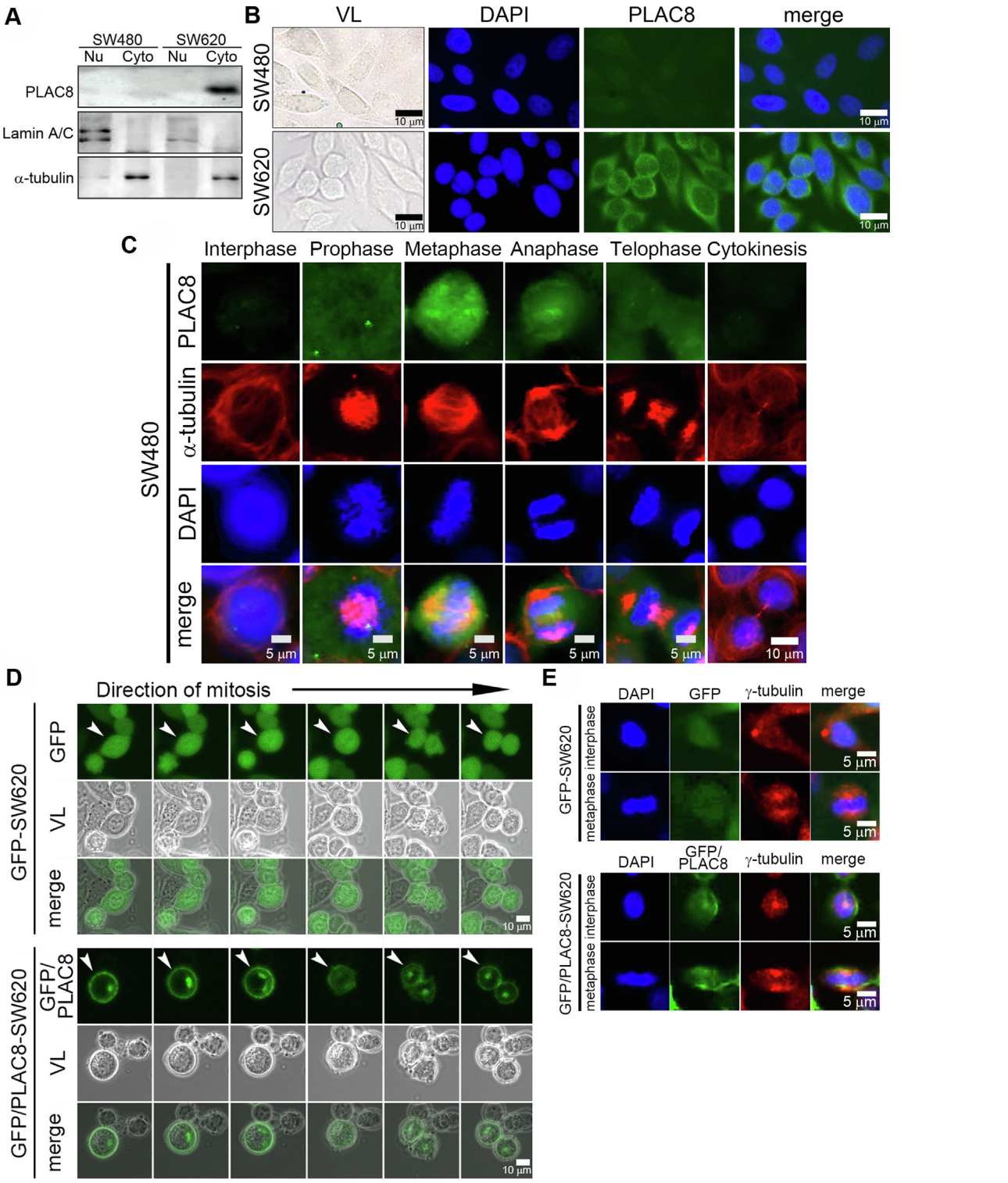

Fig. 5. Expression and translocation of PLAC8 in CRC cells undergoing cell division. (**A**) Cellular localization of PLAC8 in SW480 cells and SW620 cells. Nuclear and cytoplasmic extracts were prepared from SW480 cells and SW620 cells. Protein levels of PLAC8 were determined by Western blotting. All immunodetections used the level of Lamin A/C as a nuclear loading control and α-tubulin as a cytoplasmic loading control. (**B**) Immunofluorescent detection of PLAC8 in SW480 cells and SW620 cells. Representative images of PLAC8 (green) immunostaining. VL, visible light; DAPI, nuclear DNA (blue); merge, PLAC8 + DPAI. Scale bar, 10 μm. (**C**) Dynamic expression of PLAC8 in SW480 cells in coincidence with distinct cell cycle stages. Immunofluorescence microscopy was used to evaluate the localization of endogenously expressed PLAC8 in separate SW480 cells at distinct stages of mitosis. PLAC8, green; DAPI (nuclear DNA), blue; α-tubulin, red; merge, PLAC8 + α-tubulin + DPAI. Scale bar (5 μm), interphase, prophase, metaphase, anaphase, and telophase; scale bar (10 μm), cytokinesis. (**D**) Time-lapse images of GFP-SW620 cells and GFP/PLAC8-SW620 cells during mitosis. Images of sequential changes during mitosis were caught from the time-lapse photography. Black arrow, direction of mitosis; white arrowhead, the mitotic cells. VL, visible light. Scale bar, 10 μm. (**E**) Detection of γ-tubulin from GFP-SW620 cells and GFP/PLAC8-SW620 cells. GFP and GFP/PLAC8, green; DAPI (nuclear DNA), blue; γ-tubulin, red. Merge presented by combining green, blue and red. Scale bar, 5 μm. (For interpretation of the references to colour in this figure legend, the reader is referred to the web version of this article.)

CRC relapse or metastasis may help in identifying patients at risk of developing recurrent or metastatic CRC [39,40]. We previously found a large number of aberrant genes in human stool whose expression differed according to the clinical characteristics of CRC [13,36,41]. By accumulating sloughed cells from the colonic tract, stool provides the best opportunity for assessing CRC responses and stages, including the response to tumor therapy or CRC relapse [42]. For example, *GAS2* expression was found to be increased in the stool of recurrent CRC patients and was susceptible to chemotherapy [13]. We have also reported that the mRNA levels of *PLAC8* are increased in stool, and that its increased expression correlates with CRC relapse [12,36]. This CRC-related *PLAC8* is also upregulated in pancreatic cancer [43] or in lung cancer [44]. Therefore, it may be important to understanding the molecular significance of *PLAC8* expression in CRC tumorigenesis.

Both gene expression and gut microflora in stool can vary between healthy individuals and CRC patients [45]. As reported by Flemer et al., the CRC-associated microbiota profile differs according to disease severity, and these differences may be linked to the gene expression profile [46]. Our results seem to support the view that variations in the gut microflora might play a pivotal role in human illnesses such as CRC [47,48]. In this study, we found a low abundance of two butyrate-producing organisms in the stool of limited patients with late-stage CRC. However, this result has been verified with samples from validation group. This scenario was similar to that from Patel et al. who also used two sample groups (testing group and validation group) to target candidates [49]. An animal model was further used to validate these results from the results of H&E stain and IHC analysis of Plac8 in mouse intestinal tissues (Supplementary Fig. S2). Mouse Plac8 protein was completely absent from control intestinal tissues. The histological section from the colon of mouse without feeding *Butyricicoccus pullicaecorum* (*B. pullicaecorum*), one of butyrate-producing organisms, showed exophytic and bulky tumors, exhibiting irregular and complex dysplastic glands, to indicate intramucosal adenocarcinoma after 1,2-dimethylhydrazine (DMH) induction. Mouse with *B. pullicaecorum* administration would have the less aggressive DMH-induced CRC, which was diagnosed with several small and flat lesions ranging from low-grade adenoma to intra-epithelial carcinoma. The *B. pullicaecorum* administration made mouse with early or pre-invasive neoplasia during CRC tumorgenesis. On the other hand, our results also confirmed that butyrate negatively regulated the expression of PLAC8.

The metabolite of gut microflora, butyrate, might modulate the inflammatory response to prevent CRC [50] and PLAC8 was demonstrated in association with immunity and inflammation [51,52]. We believed that this was the first report to correlate a metabolite of gut microflora to *PLAC8* expression, which was demonstrated with oncogenic potential and cancer invasion in CRC [14]. Similarly, in the Supplementary Fig. S2, the high level of Plac8 in CRC tissue was decreased in the mice with *B. pullicaecorum* administration during the experimental process. A decrease in the number of butyrate-producing organisms and *B. longum* is common in the stool of CRC patients and may create a butyrate-deficient microenvironment. In addition to butyrate, other SCFAs have recently been reported to be produced by gut microbes in different segments of the colon [53]. Thus, understanding the gut microbiota through stool samples may be the first step to improving CRC patient health. The involvement of the gut microbiota in colorectal carcinogenesis is becoming increasingly clear [54]. Our results suggest that the lack of butyrate-producing organisms may limit lactate availability in the colonic tract [55,56]. We found that PLAC8 overexpression increased tumor growth. Moreover, tumor growth and proliferation markers were suppressed by downregulation of PLAC8 in CRC cells. Butyrate was reported with effects on multiple signaling pathways, including its inhibition on histone deacetylase (HDAC) to change some oncogenic signaling pathways [57]. We also found that butyrate could reduce the HDAC activity. If CRC cells were manipulated to express low PLAC8, butyrate could reduce more HDAC activity (Supplementary Fig. S3). These findings suggest that the negative correlation between PLAC8 expression and butyrate-producing organisms and its effects on colon cells may be crucial in CRC tumorigenesis.

Our results on gut microflora support the findings in other reports that *B. longum* and the metabolic short-chain fatty acids, specifically butyrate, could repress colonic inflammation or tumorigenesis [58,59]. This suggests that an inflammatory response may have contributed to CRC cell overgrowth by increasing PLAC8 expression and that the control of PLAC8 expression in cells might be one way to control tumor growth. We found that PLAC8 was transactivated by LPS-activated NF-κB and that this transactivation was repressed in the presence of the NF-κB inhibitor, BAY 11-7082. Roxburgh et al. reported a strong correlation between local in situ inflammation and CRC relapse [60]. However, dysbiosis of gut microflora, such as the reduction in the number of butyrate-producing organisms, was associated with gene imbalance in the colonic tract, which appeared to contribute to CRC progression.

We also found that *PLAC8* is overexpressed in most cDNA samples from tumor tissues, especially those from patients with late-stage disease. PLAC8 was more highly expressed in stage III tumor sections and was concentrated in the cytoplasm of tumor cells, which was also reported by Lee et al. [36]. Moreover, we detected that mitotic SW480 cells, which have a very low endogenous expression of PLAC8, exhibited transiently upregulated PLAC8. The results suggest that the transient expression of *PLAC8* is correlated with M phase of the cell cycle. From immunofluorescent images of SW480 cells, we also found that a strong positive signal from PLAC8 was found on the spindle poles of microtubules. In combination with the immunofluorescent results from SW620 cells, a nucleation of upregulated PLAC8 at the centrosome must correlate with mitosis and the accelerated cell proliferation. Thus, we suggest that PLAC8 is critical during the mitotic cycle and that overexpression of PLAC8 in CRC cells may contribute to increased tumor growth.

Excess PLAC8 also increases cell migration, and this molecular effect may cause tumor metastasis *in vivo*. As shown in our *in vivo* experiments in mice, CRC cells with excess PLAC8 grew faster than those with a lower level of PLAC8 expression. Importantly, after subcutaneous inoculation of PLAC8-overexpressing CRC cells into its back, a SCID mouse exhibited distant metastasis to the lung. This finding is consistent with our data from another CRC cell line, HCT 116, which has endogenously low PLAC8 expression (Supplementary Fig. S4). The overPLAC8-HCT 116 cells inoculated into the back of mice also metastasized to the lung, but RFP-HCT 116 control cells did not. These findings suggest that CRC cells with low PLAC8 expression might propagate smaller tumors that are less invasive than cells that overexpress PLAC8 [14].

We found that *PLAC8* expression in CRC cells increased with the severity of CRC. Our findings imply that downregulation of *PLAC8* in CRC may alter the expression of proliferation genes, which might slow the growth and migration of CRC cells. Therefore, controlling the expression of PLAC8 with anti-inflammatory agents or treating cells with butyrate might reduce the PLAC8-induced malignant effects. Activation of the inflammatory response or dysbiosis of target microflora may increase PLAC8 expression, which may contribute to advanced or recurrent CRC. We also found that butyrate induced an apoptotic effect in CRC cells with upregulated expression of *PLAC8*, a finding contradicting the known anti-apoptotic effect of PLAC8 in other cell types [43].

Conclusions

In conclusion, our study of the relationships between PLAC8, butyrate, and tumor progression indicate that PLAC8 expression and butyrate-producing microorganisms are critical to the growth and migration of CRC cells [61]. Other gut bacteria, such as *Bifidobacterium*, may also have clinical significance in CRC. A metabolite of butyrate-producing microorganisms reduced the expression of PLAC8 in colon cells and therefore might have clinical significance. Our results also suggest that PLAC8 expression might be an indicator of CRC progression and dysbiosis of the gut microflora, especially dysbiosis of butyrate-producing microorganisms.

Compliance with Ethics Requirements

All Institutional and National Guidelines for the care and use of animals (The Animal Care Committee of Cathay General Hospital, Taiwan) were followed.

Declaration of Competing Interest

The authors have declared no conflict of interest.

Acknowledgements

This study was funded by Ministry of Science and Technology, Taiwan (grant numbers MOST104-2314-B-281-004-MY2 and MOST106-2314-B-281-007 to CJH). This study was also supported by Cathay General Hospital, Taiwan (grant numbers CGH-MR-A10317 to CJH, CGH- MR-A10312 to CCH, and CGH-MR-A10512 to MHS). We thank Dr. Wei-Chi Ku (College of Medicine, Fu Jen Catholic University) for English corrections that help improving the manuscript as well as his constructive comments. We also thank Dr. Yu-Lun Kuo (Biotools Co., New Taipei, Taiwan) for his professional bioinformatics in analyzing microbiota and Mr. Tsan-Jhu Chen (Institute of Nuclear Energy Research, Taoyuan, Taiwan) for providing the superior technique in analyzing the images of nanoPET/CT.

Appendix A. Supplementary material

Supplementary data to this article can be found online at https://doi.org/10.1016/j.jare.2019.11.005.

References

[1] Arnold M, Sierra MS, Laversanne M, Soerjomataram I, Jemal A, Bray F. Global patterns and trends in colorectal cancer incidence and mortality. Gut 2017;66(4):683–91.
[2] Siegel RL, Miller KD, Jemal A. Cancer statistics, 2019. CA Cancer J Clin 2019;69(1):7–34.
[3] Clark CR, Starr TK. Mouse models for the discovery of colorectal cancer driver genes. World J Gastroenterol 2016;22(2):815–22.
[4] Takakura Y, Ikeda S, Imaoka Y, Urushihara T, Itamoto T. An elevated preoperative serum carbohydrate antigen 19–9 level is a significant predictor for peritoneal dissemination and poor survival in colorectal cancer. Colorectal Dis 2015;17(5):417–25.
[5] Duineveld LA, van Asselt KM, Bemelman WA, Smits AB, Tanis PJ, van Weert HC, et al. Symptomatic and asymptomatic colon cancer recurrence: a multicenter cohort study. Ann Fam Med 2016;14(3):215–20.
[6] Tokodai K, Narimatsu H, Nishida A, Takaya K, Hara Y, Kawagishi N, et al. Risk factors for recurrence in stage II/III colorectal cancer patients treated with curative surgery: The impact of postoperative tumor markers and an infiltrative growth pattern. J Surg Oncol 2016;114(3):368–74.
[7] Konishi T, Shimada Y, Lee LH, Cavalcanti MS, Hsu M, Smith JJ, et al. Poorly differentiated clusters predict colon cancer recurrence: an in-depth comparative analysis of invasive-front prognostic markers. Am J Surg Pathol 2018;42(6):705–14.
[8] You JS, Jones PA. Cancer genetics and epigenetics: two sides of the same coin?. Cancer Cell 2012;22(1):9–20.
[9] Boland CR, Goel A. Prognostic subgroups among patients with stage II colon cancer. N Engl J Med 2016;374(3):277–8.
[10] Tsai HL, Huang CW, Chen CW, Yeh YS, Ma CJ, Wang JY. Survival in resected stage II colorectal cancer is dependent on tumor depth, vascular invasion, postoperative CEA level, and the number of examined lymph nodes. World J Surg 2016;40(4):1002–9.
[11] Huang CJ, Yang SH, Huang SM, Lin CM, Chien CC, Chen YC, et al. A predicted protein, KIAA0247, is a cell cycle modulator in colorectal cancer cells under 5-FU treatment. J Transl Med 2011;9:82.
[12] Chang CC, Huang CC, Yang SH, Chien CC, Lee CL, Huang CJ. Data on clinical significance of GAS2 in colorectal cancer cells. Data Brief 2016;8:82–6.
[13] Huang CJ, Lee CL, Yang SH, Chien CC, Huang CC, Yang RN, et al. Upregulation of the growth arrest-specific-2 in recurrent colorectal cancers, and its susceptibility to chemotherapy in a model cell system. Biochim Biophys Acta 2016;1862(7):1345–53.
[14] Li C, Ma H, Wang Y, Cao Z, Graves-Deal R, Powell AE, et al. Excess PLAC8 promotes an unconventional ERK2-dependent EMT in colon cancer. J Clin Invest 2014;124(5):2172–87.
[15] Wang T, Cai G, Qiu Y, Fei N, Zhang M, Pang X, et al. Structural segregation of gut microbiota between colorectal cancer patients and healthy volunteers. ISME J 2012;6(2):320–9.
[16] Wang Y, Huang D, Chen KY, Cui M, Wang W, Huang X, et al. Fucosylation deficiency in mice leads to colitis and adenocarcinoma. Gastroenterology 2017;152(1):193–205. e10.
[17] Rezasoltani S, Asadzadeh-Aghdaei H, Nazemalhosseini-Mojarad E, Dabiri H, Ghanbari R, Zali MR. Gut microbiota, epigenetic modification and colorectal cancer. Iran J Microbiol 2017;9(2):55–63.
[18] Wang X, Yang Y, Huycke MM. Commensal-infected macrophages induce dedifferentiation and reprogramming of epithelial cells during colorectal carcinogenesis. Oncotarget 2017;8(60):102176–90.
[19] Mima K, Ogino S, Nakagawa S, Sawayama H, Kinoshita K, Krashima R, et al. The role of intestinal bacteria in the development and progression of gastrointestinal tract neoplasms. Surg Oncol 2017;26(4):368–76.
[20] Wu X, Wu Y, He L, Wu L, Wang X, Liu Z. Effects of the intestinal microbial metabolite butyrate on the development of colorectal cancer. J Cancer 2018;9(14):2510–7.
[21] Jensen MM, Erichsen KD, Bjorkling F, Madsen J, Jensen PB, Hojgaard L, et al. Early detection of response to experimental chemotherapeutic Top216 with [18F]FLT and [18F]FDG PET in human ovary cancer xenografts in mice. PLoS One 2010;5(9):e12965.
[22] Magoč T, Salzberg SL. FLASH: fast length adjustment of short reads to improve genome assemblies. Bioinformatics 2011;27(21):2957–63.
[23] Caporaso JG, Kuczynski J, Stombaugh J, Bittinger K, Bushman FD, Costello EK, et al. QIIME allows analysis of high-throughput community sequencing data. Nat Methods 2010;7(5):335–6.
[24] Bokulich NA, Subramanian S, Faith JJ, Gevers D, Gordon JI, Knight R, et al. Quality-filtering vastly improves diversity estimates from Illumina amplicon sequencing. Nat Methods 2013;10(1):57–9.
[25] Edgar RC, Haas BJ, Clemente JC, Quince C, Knight R. UCHIME improves sensitivity and speed of chimera detection. Bioinformatics 2011;27(16):2194–200.
[26] Haas BJ, Gevers D, Earl AM, Feldgarden M, Ward DV, Giannoukos G, et al. Chimeric 16S rRNA sequence formation and detection in Sanger and 454-pyrosequenced PCR amplicons. Genome Res 2011;21(3):494–504.
[27] Edgar RC. Search and clustering orders of magnitude faster than BLAST. Bioinformatics 2010;26(19):2460–1.
[28] Edgar RC. UPARSE: highly accurate OTU sequences from microbial amplicon reads. Nat Methods 2013;10(10):996–8.
[29] DeSantis TZ, Hugenholtz P, Larsen N, Rojas M, Brodie EL, Keller K, et al. Greengenes, a chimera-checked 16S rRNA gene database and workbench compatible with ARB. Appl Environ Microbiol 2006;72(7):5069–72.
[30] McDonald D, Price MN, Goodrich J, Nawrocki EP, DeSantis TZ, Probst A, et al. An improved Greengenes taxonomy with explicit ranks for ecological and evolutionary analyses of bacteria and archaea. The ISME J 2012;6(3):610.
[31] Caporaso JG, Bittinger K, Bushman FD, DeSantis TZ, Andersen GL, Knight R. PyNAST: a flexible tool for aligning sequences to a template alignment. Bioinformatics 2009;26(2):266–7.
[32] White JR, Nagarajan N, Pop M. Statistical methods for detecting differentially abundant features in clinical metagenomic samples. PLoS Comput Biol 2009;5(4):e1000352.
[33] Jiang X-T, Peng X, Deng G-H, Sheng H-F, Wang Y, Zhou H-W, et al. Illumina sequencing of 16S rRNA tag revealed spatial variations of bacterial communities in a mangrove wetland. Microb Ecol 2013;66(1):96–104.
[34] Xu T, Xiao D, Zhang X. ECRG4 inhibits growth and invasiveness of squamous cell carcinoma of the head and neck in vitro and in vivo. Oncol Lett 2013;5(6):1921–6.
[35] Jensen MM, Jorgensen JT, Binderup T, Kjaer A. Tumor volume in subcutaneous mouse xenografts measured by microCT is more accurate and reproducible than determined by 18F-FDG-microPET or external caliper. BMC Med Imaging 2008;8:16.
[36] Lee CL, Huang CJ, Yang SH, Chang CC, Huang CC, Chien CC, et al. Discovery of genes from feces correlated with colorectal cancer progression. Oncol Lett 2016;12(5):3378–84.
[37] Zhang LJ, Pan B, Chen B, Zhang XF, Liang GJ, Feng YN, et al. Expression and epigenetic dynamics of transcription regulator Lhx8 during mouse oogenesis. Gene 2012;506(1):1–9.

[38] Maus MK, Hanna DL, Stephens CL, Astrow SH, Yang D, Grimminger PP, et al. Distinct gene expression profiles of proximal and distal colorectal cancer: implications for cytotoxic and targeted therapy. Pharmacogenomics J 2015;15(4):354–62.
[39] Hardingham JE, Grover P, Winter M, Hewett PJ, Price TJ, Thierry B. Detection and clinical significance of circulating tumor cells in colorectal cancer–20 years of progress. Mol Med 2015;21(Suppl 1):S25–31.
[40] Chand M, Keller DS, Mirnezami R, Bullock M, Bhangu A, Moran B, et al. Novel biomarkers for patient stratification in colorectal cancer: A review of definitions, emerging concepts, and data. World J Gastrointest Oncol 2018;10(7):145–58.
[41] Huang CJ, Yang SH, Lee CL, Cheng YC, Tai SY, Chien CC. Ribosomal protein S27-like in colorectal cancer: a candidate for predicting prognoses. PLoS One 2013;8(6):e67043.
[42] de Wijkerslooth TR, Bossuyt PM, Dekker E. Strategies in screening for colon carcinoma. Neth J Med 2011;69(3):112–9.
[43] Mourtada-Maarabouni M, Watson D, Munir M, Farzaneh F, Williams GT. Apoptosis suppression by candidate oncogene PLAC8 is reversed in other cell types. Curr Cancer Drug Targets 2013;13(1):80–91.
[44] Jia Y, Ying X, Zhou J, Chen Y, Luo X, Xie S, et al. The novel KLF4/PLAC8 signaling pathway regulates lung cancer growth. Cell Death Dis 2018;9(6):603.
[45] Wong SH, Zhao L, Zhang X, Nakatsu G, Han J, Xu W, et al. Gavage of fecal samples from patients with colorectal cancer promotes intestinal carcinogenesis in germ-free and conventional mice. Gastroenterology 2017;153(6). pp. 1621–33 e6.
[46] Flemer B, Lynch DB, Brown JM, Jeffery IB, Ryan FJ, Claesson MJ, et al. Tumour-associated and non-tumour-associated microbiota in colorectal cancer. Gut 2017;66(4):633–43.
[47] Dai Z, Zhang J, Wu Q, Chen J, Liu J, Wang L, et al. The role of microbiota in the development of colorectal cancer. Int J Cancer 2019;145(8):2032–41.
[48] Khan S, Imran A, Malik A, Chaudhary AA, Rub A, Jan AT, et al. Bacterial imbalance and gut pathologies: Association and contribution of E. coli in inflammatory bowel disease. Crit Rev Clin Lab Sci 2019;56(1):1–17.
[49] Patel MJ, Bell CS, Lally KP, Lally PA, Katakam LI. Congenital Diaphragmatic Hernia Study G. Lowest PaCO2 on the first day of life predicts mortality and morbidity among infants with congenital diaphragmatic hernia. J Perinatol 2019;39(2):229–36.
[50] Chen J, Vitetta L. Inflammation-Modulating effect of butyrate in the prevention of colon cancer by dietary fiber. Clin Colorectal Cancer 2018;17(3):e541–4.
[51] McHugh L, Seldon TA, Brandon RA, Kirk JT, Rapisarda A, Sutherland AJ, et al. A molecular host response assay to discriminate between sepsis and infection-negative systemic inflammation in critically Ill patients: discovery and validation in independent cohorts. PLoS Med 2015;12(12):e1001916.
[52] Johnson RM, Kerr MS, Slaven JE. Plac8-dependent and inducible NO synthase-dependent mechanisms clear Chlamydia muridarum infections from the genital tract. J Immunol 2012;188(4):1896–904.
[53] Neis EP, van Eijk HM, Lenaerts K, Olde Damink SW, Blaak EE, Dejong CH, et al. Distal versus proximal intestinal short-chain fatty acid release in man. Gut 2019;68(4):764–5.
[54] Gagniere J, Raisch J, Veziant J, Barnich N, Bonnet R, Buc E, et al. Gut microbiota imbalance and colorectal cancer. World J Gastroenterol 2016;22(2):501–18.
[55] Bourriaud C, Robins RJ, Martin L, Kozlowski F, Tenailleau E, Cherbut C, et al. Lactate is mainly fermented to butyrate by human intestinal microfloras but inter-individual variation is evident. J Appl Microbiol 2005;99(1):201–12.
[56] Wang G, Yu Y, Wang YZ, Wang JJ, Guan R, Sun Y, et al. Role of SCFAs in gut microbiome and glycolysis for colorectal cancer therapy. J Cell Physiol 2019;234(10):17023–49.
[57] Chen J, Zhao KN, Vitetta L. Effects of intestinal microbial(-)elaborated butyrate on oncogenic signaling pathways. Nutrients 2019;11(5). pii: E1026.
[58] Datta S, Chowdhury S, Roy HK. Metabolism, microbiome and colorectal cancer. Aging (Albany NY) 2017;9(4):1086–7.
[59] Eslami M, Yousefi B, Kokhaei P, Hemati M, Nejad ZR, Arabkari V, et al. Importance of probiotics in the prevention and treatment of colorectal cancer. J Cell Physiol 2019;234(10):17127–43.
[60] Roxburgh CS, McMillan DC. The role of the in situ local inflammatory response in predicting recurrence and survival in patients with primary operable colorectal cancer. Cancer Treat Rev 2012;38(5):451–66.
[61] Devriese S, Eeckhaut V, Geirnaert A, Van den Bossche L, Hindryckx P, Van de Wiele T, et al. Reduced Mucosa-associated butyricicoccus activity in patients with ulcerative colitis correlates with aberrant Claudin-1 expression. J Crohns Colitis 2017;11(2):229–36.